INTERNATIONAL JOURNAL FOR NUMERICAL AND ANALYTICAL METHODS IN GEOMECHANICS
Int. J. Numer. Anal. Meth. Geomech., **23**, 187–215 (1999)

FINITE ELEMENT ANALYSIS FOR A FINITE CONDUCTIVITY FRACTURE IN AN INFINITE POROELASTIC MEDIUM

Y.-C. LI*

Department of Civil Engineering, Shanghai Tiedao University, Shanghai 200331, People's Republic of China

SUMMARY

In the technology of oil recovery, oil production rate can be increased by generation of a vertical conductive fracture adjacent to the well-bore. In this paper the seepage flow and isothermal deformation in both the oil formation and the fracture are studied by modelling the formation as a two-dimensional infinite poroelastic medium and the conductive fracture as a one-dimensional poroelastic material, saturated by a one-phase compressible fluid. The plane strain condition is employed. Solutions for a growing conductive fracture and a stationary conductive fracture in the infinite medium are obtained by means of the finite element method based on a variational principle for the formation which can impose the governing equations of the fracture. Infinite elements are used outside the finite element domain. Numerical results indicate that the injection rate, the applied pressure and the crack mouth opening displacement at the well-bore oscillate during the propagation of the conductive fracture. The production rate of a well with the conductive fracture is compared with that of a well without the conductive fracture. Finally, a new definition of the conductivity coefficient for the conductive fracture is presented. Copyright © 1999 John Wiley & Sons, Ltd.

Key words: finite element; conductive fracture; growing; poroelastic, infinite; well-bore

INTRODUCTION

Analysis of the flow field in an oil-bearing formation near a production well is important in the study of hydraulic fracture growth and in determination of the relationship between the oil production rate and the applied pressure at the well-bore during oil recovery. When the permeability of the formation is low, a hydraulic fracturing technique can be used to increase the production rate. In this technique, a high pressure is applied to the production well through the injected fluid to generate a crack. The injected fluid carries highly permeable material such as sand, which displaces into the crack with the fluid. As the applied pressure is removed, the sand remains in the crack to form a band of sand which keeps the crack open. The production rate can be raised due to the increase in diffusive area from the conductive fracture. In the engineering practice of oil recovery, the territories of the pay-zones may extend far beyond the production

*Correspondence to: Y.-C. Li, Department of Civil Engineering, Shanghai Tiedao University, Shanghai 200333, People's Republic of China

Contract grant number: Science Foundation G95 (02); contract grant sponsor: State Education Commission, People's Republic of China

CCC 0363–9061/99/030187–29$17.50

Received 24 February 1997
Revised 5 March 1998

wells and the regions to be analyzed are of small dimension in comparison with the pay-zones. In this case, these pay-zones can be naturally idealized as infinite media.

Consider a model of plane strain consisting of a conductive fracture in an infinitely large poroelastic medium with the production well located at the centre of the fracture. Several exact and approximate analytical solutions for this model have been presented for determination of the effect of the conductive fracture on well performance and transient pressure behaviour. In these solutions the influence of the deformation of the medium on the seepage in the medium is neglected. The size of the well diameter is omitted in comparison with the length of the conductive fracture. Gringarten *et al.*[1] found three basic solutions: (i) the infinite fracture conductivity solution associated with the uniformly distributed applied pressure along a fully penetrating vertical fracture, (ii) the uniform flux solution for a fully penetrating vertical fracture and (iii) the uniform flux solution for a horizontal fracture. Kucuk and Brigham[2] presented the analytical solutions for the problem of a slot located in an infinite medium with a prescribed constant pressure on the slot surface and the problem with a prescribed constant flow rate in the slot (hereafter referred to as 'Kucuk's problem'). With the use of Green's function, Cinco-Ley *et al.*[3] developed a semi-analytical method to estimate the solution for the problem of a rectangular finite conductivity fracture in an infinite medium (hereafter referred to as 'Cinco–Ley's problem'). Recently, Li[4] found approximate analytical solutions for Kucuk's problem. Based on these approximate solutions, he developed a type of highly efficient infinite elements to simulate the transient pressure behavior outside the finite element domain. His numerical solutions are proved accurate compared with Kucuk's and Cinco-Ley's solutions. Numerical solutions for deformation/seepage coupled problems were presented by Li and Huang.[5] They extrapolated a series of finite element solutions for finite media to estimate the solution for the infinite medium.

Several authors studied the problem of a growing crack with an infinite fracture conductivity in an infinite poroelastic medium. The crack is full of water without the band of sand. Either the internal pressure is uniformly distributed on the crack surface or the fluid flow in the growing crack is governed by some kind of fluid flow equation such as the Navier–Stokes equation for a one-dimensional flow. Self-similarity solution of the hydraulic fracture growth with an impermeable crack surface was studied by Spence and Sharp[6] and by Huang *et al.*[7]. Non-similarity solution of the hydraulic fracturing problem with an impermeable crack surface was studied by Huang and Li.[8] Either inviscid or viscous flow in the fracture was considered in their work. An analysis of the general three-dimensional planar fracture growth under a specific spectrum of a well-bore pressure was done by Lam and Cleary.[9] A numerical procedure for approximation to a two-dimensional, hydraulically driven fracture propagation in a porous medium was developed by Boone and Ingraffea.[10] In their work, the viscous flow in the fracture was modeled by a finite difference approximation. An equilibrium fracture model based on a generalized Dugdale–Barenblatt concept was used to determine the fracture dimension. However, studies for simulating the deformation and seepage fields for propagation of a finite conductivity crack in an infinite poroelastic medium have not yet been published thus far.

In this paper, problems of a single production well with a finite conductivity fracture in an infinite poroelastic medium are studied. In the present theoretical modal, the oil formation is constrained at the top and the bottom by rigid and impermeable strata. No friction exists between the formation and the strata. Both the production well and the conductive crack are penetrating and vertical. The crack is planar and has a straight front. The thickness of the medium is assumed to be so large that a plane strain mode can be employed. A short crack connected to the well-bore exists initially. The crack is forced to propagate by the fluid injected under a high pressure, and is

filled with sand simultaneously. When the crack reaches a desired length, the applied pressure will be removed. A sustained conductive fracture is thus formed in the medium. The oil in the formation will flow back through the surface of the sustained fracture to the production well. We shall simulate the displacement and transient pressure fields and calculate the flow rate at the production well for this entire procedure. The differential equation for diffusion in the growing conductive crack will be developed. The governing equations for a growing conductive crack and a sustained stationary conductive crack will be imposed in the variational principle of the formation for establishing the finite element equations.

GOVERNING EQUATIONS AND A VARIATIONAL PRINCIPLE

For a poroelastic medium

Consider a homogeneous and isotropic poroelastic medium saturated with a single phase compressible fluid and subjected to a small deformation. The governing equations for a three-dimensional isothermal medium were given by Biot[11] as follows:

Strain–displacement relations

$$\varepsilon_{ij} = \tfrac{1}{2}(u_{i,j} + u_{j,i}) \tag{1}$$

Equilibrium equations:

$$\sigma_{ij,j} = 0 \tag{2}$$

Constitutive relations:

$$\sigma_{ij} = H_{ijkl}\varepsilon_{kl} - \lambda p\delta_{ij} \tag{3}$$

$$cp = \zeta - \lambda\varepsilon_{ii} \tag{4}$$

Continuity equation:

$$\dot{\zeta} + v_{i,i} = 0 \tag{5}$$

Darcy's law:

$$v_i = -Kp_{,i} \tag{6}$$

These equations are written in indexical notations. Summation is implied for repeated indices. In these equations, u_i is the displacement vector, ε_{ij} is the solid strain tensor, ε_{ii} is the volumetric strain, σ_{ij} is the total stress tensor, p is the pore pressure, ζ is the increase in fluid volume per unit reference volume, v_i is the specific discharge vector, K is the permeability coefficient, c is the storage coefficient, λ is the Biot's effective stress coefficient, H_{ijkl} is the stress–strain relation tensor, δ is the Kronecker delta, $(\ )_{,i} = \partial(\ )/\partial x_i$ and $\dot{(\ )} = \partial(\ )/\partial t$. Note that the body forces of the medium and the fluid are ignored. The permeability coefficient K is related to the intrinsic permeability k of the medium by

$$K = \frac{k}{\phi\mu} \tag{7}$$

where ϕ is the porosity of the medium and μ is the dynamic viscosity of the fluid. For an isotropic medium, the stress–strain relation tensor H_{ijkl} can be expressed by

$$H_{ijkl} = 2G\left(\delta_{ik}\delta_{jl} + \frac{\nu}{1-2\nu}\,\delta_{ij}\delta_{kl}\right) \tag{8}$$

where G is the shear modulus of the medium and v is the Poisson's ratio of the medium. The Biot's effective stress coefficient λ and the storage coefficient c can be respectively expressed by

$$\lambda = \frac{3(v_u - v)}{B(1 - 2v)(1 + v_u)} \tag{9}$$

$$c = \frac{9(1 - 2v_u)(v_u - v)}{2GB^2(1 - 2v)(1 + v_u)^2} \tag{10}$$

where B is the Skempton pore pressure coefficient, v and v_u are the drained and undrained Poisson's ratios, respectively. It is observed that a set of five material parameters, say G, v, v_u, B and K, completely define the system. For the convenience of future reference, we also define a generalized consolidation coefficient

$$C = \frac{2KB^2G(1 - v)(1 + v_u)^2}{9(1 - v_u)(v_u - v)} \tag{11}$$

Generally, C can replace K in the basic set of the material constants.

It may be worthwhile to mention a specialized case of incompressible constituents of solid and fluid. This special case can be accommodated by setting the material parameters $v_u = 0{\cdot}5$ and $B = 1$, which leads to $\lambda = 1$ and $c = 0$.

Equations (4)–(6) can be combined into

$$-Kp_{,ii} + \lambda\dot{\varepsilon}_{ii} + c\dot{p} = 0 \tag{12}$$

Note that if $\lambda = 0$, equation (12) is reduced to a typical diffusion equation of the pore pressure and the problem becomes an uncoupled one.

The porous medium occupies a volume V with a surface S. The boundary conditions are

$$u_i = u_i^* \quad \text{on } S_u \tag{13a}$$

$$\sigma_{ij}n_j = P_i^* \quad \text{on } S_\sigma \tag{13b}$$

$$p = p^* \quad \text{on } S_p \tag{13c}$$

$$v_i n_i = V_n^* \quad \text{on } S_v \tag{13d}$$

where $S_u + S_\sigma = S_p + S_v = S$, n_i is the outward unit normal to the surface, u_i^* is the prescribed displacement, P_i^* is the prescribed surface traction, p^* is the prescribed pore pressure, V_n^* is the prescribed normal flow rate. These quantities are regarded as time dependent. Assuming that the boundary conditions are applied gradually, the initial conditions at $t = 0^+$ are

$$u_i(x_1, x_2, x_3; 0^+) = 0 \tag{14a}$$

$$\zeta(x_1, x_2, x_3; 0^+) = 0 \tag{14b}$$

$$p(x_1, x_2, x_3; 0^+) = 0 \tag{14c}$$

Let us use a two-step backward finite difference equation with variable time increments to approximate the time derivative in equation (12), i.e.

$$(\dot{\ }) = a_0(\ ) + a_{-1}(\ )_{-1} + a_{-2}(\ )_{-2} \tag{15}$$

where

$$a_0 = \frac{2\Delta_{-1} + \Delta_{-2}}{\Delta_{-1}(\Delta_{-1} + \Delta_{-2})}, \quad a_{-1} = -\frac{\Delta_{-1} + \Delta_{-2}}{\Delta_{-1}\Delta_{-2}}, \quad a_{-2} = \frac{\Delta_{-1}}{\Delta_{-2}(\Delta_{-1} + \Delta_{-2})} \tag{16}$$

are three coefficients depending on the two-backward time increments Δ_{-1} and Δ_{-2}. Subscripts -1 and -2 denote the values of the field quantities at time $t - \Delta_{-1}$ and $t - \Delta_{-1} - \Delta_{-2}$, respectively. Let us consider the following functional:

$$\begin{aligned}\Phi = &\int_V \left(\frac{1}{2} H_{ijkl}\varepsilon_{ij}\varepsilon_{kl} - \lambda p\varepsilon_{ii} - \frac{K}{2a_0} p_{,i}p_{,i} - \frac{c}{2} p^2\right) \mathrm{d}V \\ &- \int_V \frac{1}{a_0} \lambda p[a_{-2}(\varepsilon_{ii})_{-2} + a_{-1}(\varepsilon_{ii})_{-1}] \,\mathrm{d}V \\ &- \int_V \frac{1}{a_0} cp\,[a_{-2}p_{-2} + a_{-1}p_{-1}] \,\mathrm{d}V \\ &- \int_{S_\sigma} P_i^* u_i \,\mathrm{d}S - \int_{S_v} \frac{1}{a_0} V_n^* p \,\mathrm{d}S \end{aligned} \tag{17}$$

It can be shown that among all u_i and p which satisfy the strain–displacement relations, equation (1) and the boundary conditions, equations (13a) and (13c), the actual solution of u_i and p for equations (2), (3) and (12) will make Φ stationary, i.e. the first variation of Φ satisfies

$$\delta\Phi = 0 \tag{18}$$

Equations (17) and (18) form a variational principle for displacement/pressure coupled problems in poroelastic media. Several authors presented variational principles for the coupled problems in different ways. Ghaboussi and Wilson[13] presented the variational principles for coupled problems using convolution integrals. In their method, after the finite element equations are generated, time domain is discretized for execution of the convolution integral with respect to time. Huang *et al.*[12] presented variational principles for problems coupled by displacement, pore pressure and temperature in poroelastic media. In their method, the Laplace transform is introduced and the time derivatives in the governing equations are shifted to an integral form multiplied by a transform parameter. Their variational functionals are then based on the Laplace transformed quantities. When the finite element equations are formed from the variational principles, an inverse Laplace transform is taken and the time derivatives appear again in these equations. Afterward, the time derivatives are approximated by finite difference. However, in our method, the time domain is discretized before establishing the variational principles. In the next section for finite element discretization, it will be found that the finite element equations resulting from our variational principle are the same as those presented by Huang *et al.*[12].

For a plane strain problem, the foregoing governing equations and variational functional still hold, but all material constants should be replaced by the corresponding quantities in the plane strain case.[12] The volume integrals and surface integrals should be replaced by the area integrals and contour integrals respectively.

In addition, we need a criterion for crack growth in the poroelastic medium. During crack propagation, the transient stress intensity factor for the opening model $K_I(t)$ is maintained at

a level of K_{IC}, i.e.

$$K_I(t) = K_{IC} \tag{19}$$

where K_{IC} is the fracture toughness of the medium in the opening mode, which is considered to be a material constant and independent of the crack length.

For a growing conductive fracture

When the pressure applied on the injected fluid is higher than the *in-situ* stress, an initial fracture can be generated and the fracture will propagate thereafter. The sand in the fluid will fill the fracture, and a conductive fracture will be formed. During the propagation of the conductive fracture, the sand in the fracture is accumulated without deformation in the band of sand. Hence, the governing equation for diffusion in the conductive fracture under a plane strain condition can be expressed by

$$-K_{\mathrm{f}}(p_{,1}\, b_{\mathrm{f}})_{,1} + \phi_{\mathrm{f}}\dot{b}_{\mathrm{f}} + c_{\mathrm{f}} b_{\mathrm{f}}\dot{p} + 2v_n = 0 \tag{20}$$

where K_{f} is the permeability coefficient of the material in the conductive fracture, ϕ_{f} is the porosity of the material, c_{f} is the storage coefficient of the material, b_{f} is the width of the conductive fracture, v_n is the specific leak-off discharge vector through the fracture surface which is prescribed positive for fluid flow from the conductive fracture into the medium. The fracture is located on the x_1-axis with the centre at the origin. Since the fracture width is narrow compared with the fracture length, a linear flow in the fracture can be considered. Furthermore, it can be assumed that the pore pressure p and the specific discharge $v_1 = -K_{\mathrm{f}}p_{,1}$ is uniformly distributed on the cross section of the conductive fracture. Description of equation (20) is shown in Figure 1. In fact, equation (20) is a combination of the diffusion equation in the conductive fracture with the increase of the width of the fracture during the crack propagation.

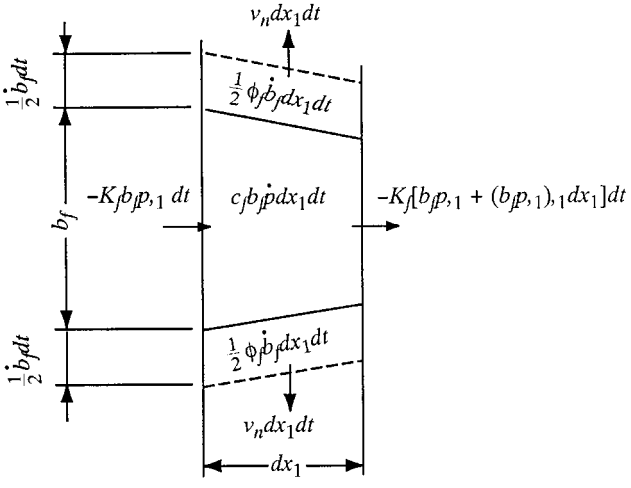

Figure 1. Illustration of the diffusion equation for a growing conductive crack

Let us consider the variational form of the last integral in equation (17). Since crack surface is the only boundary for infinite medium under plane strain condition, we have

$$\delta\Pi_g = \delta \int_{S_v} \frac{1}{a_0} V_n^* p \, \mathrm{d}s = \int_0^{L(t)} \frac{1}{a_0} V_n^* \delta p \, \mathrm{d}x_1 \tag{21}$$

where $L(t)$ is the transient semi-crack length. Note that $V_n^* = -v_n$. Eliminating V_n^* and v_n from equations (20) and (21), we obtain

$$\delta\Pi_g = \frac{1}{2a_0} \left\{ -[K_f b_f p_{,1} \delta p]_0^{L(t)} + K_f \int_0^{L(t)} b_f p_{,1} \delta p_{,1} \, \mathrm{d}x_1 + \phi_f \int_0^{L(t)} \dot{b}_f \delta p \, \mathrm{d}x_1 + c_f \int_0^{L(t)} b_f \dot{p} \delta p \, \mathrm{d}x_1 \right\} \tag{22}$$

where the approach of integral by parts is utilized. Note that $-K_f b_f p_{,1} = 0{\cdot}5 q_w$ at the well-bore and b_f vanishes at the crack tip, where q_w is the total flow rate at the well-bore and is defined positive for flowing from the well-bore into the fracture. Thus equation (22) becomes

$$\delta\Pi_g = \frac{1}{2a_0} \left[0{\cdot}5 q_w \delta p_w + K_f \int_0^{L(t)} b_f p_{,1} \delta p_{,1} \, \mathrm{d}x_1 + \phi_f \int_0^{L(t)} \dot{b}_f \delta p \, \mathrm{d}x_1 + c_f \int_0^{L(t)} b_f \dot{p} \delta p \, \mathrm{d}x_1 \right] \tag{23}$$

where p_w is the applied pressure at the well-bore.

For a stationary conductive fracture

As the applied pressure is removed, the crack growth will be stopped and the sand carried by the fluid will remain in the formation to form a stationary conductive fracture. The stationary fracture is located on the x_1-axis from $x_1 = -L$ to $x_1 = L$. The governing equations (1)–(6) still hold in the conductive fracture, but all material constants are denoted by adding a subscript 'f' referring to the constants of the material in the fracture. Since the crack is narrow, the strain components ε_{11} and ε_{12} can be neglected in comparison with the transverse normal strain ε_{22}. Correspondingly, the stress components σ_{11} and σ_{12} can also be neglected. Thus, the constructive relations (3) and (4) and the Darcy's law (6) are reduced to

$$\sigma_{22} + \lambda_f p = E_f \varepsilon_{22} \tag{24}$$

$$\zeta = \lambda_f \varepsilon_{22} + c_f p \tag{25}$$

$$v_1 = -K_f p_{,1} \tag{26}$$

where E_f is the Young's modulus of the material in the conductive fracture. After integration of the continuity equation (5) through the width of the crack, we obtain

$$v_{1,1} b_f + \dot{\zeta} b_f + 2v_n = 0 \tag{27}$$

Equations (25)–(27) can be combined into

$$-K_f b_f p_{,11} + \lambda_f b_f \dot{\varepsilon}_{22} + c_f b_f \dot{p} + 2v_n = 0 \tag{28}$$

If the upper half-plane is taken into consideration (Figure 2), the traction on the fracture surface is $T_2 = -\sigma_{22}$. Since the change in b_f with time is small, the value of b_f in equation (28) can be approximately replaced by a time independent value b_{f0}, which is the width of the growing conductive fracture when the growth is terminated, as well as the initial width of the sustained

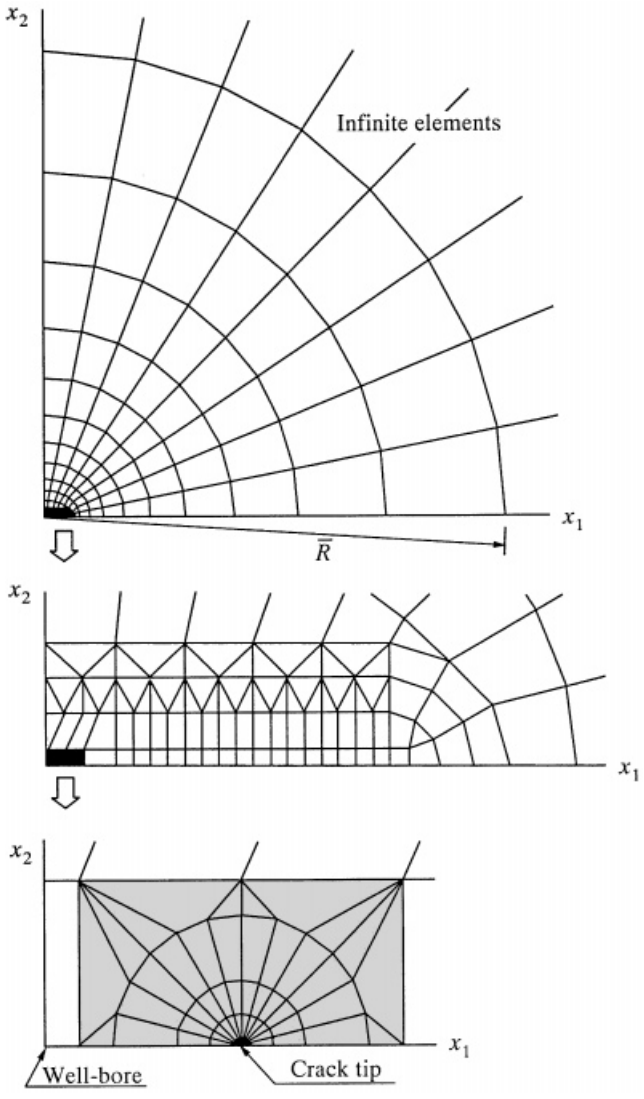

Figure 2. Finite element layout for the example problem

stationary conductive fracture also. The transverse strain can be expressed by

$$\varepsilon_{22} = \frac{b_f - b_{f0}}{b_{f0}} \tag{29}$$

Equations (24) and (28) then become

$$-T_2 + \lambda_f p = E_f \frac{b_f - b_{f0}}{b_{f0}} \tag{30}$$

$$-K_f b_{f0} p_{,11} + \lambda_f \dot{b}_f + c_f b_{f0} \dot{p} + 2v_n = 0 \tag{31}$$

Equation (31) can be imposed into the variational principle. The variational form of the last integral in equation (17) can be written as

$$\delta\Pi_s = \delta\int_{S_v}\frac{1}{a_0}V_n^* p\,\mathrm{d}S = \int_0^L \frac{1}{a_0}V_n^*\,\delta p\,\mathrm{d}x_1$$
$$= \frac{1}{2a_0}\left[0{\cdot}5q_w\delta p_w + K_f\int_0^L b_{f0}p_{,1}\delta p_{,1}\,\mathrm{d}x_1 + \lambda_f\int_0^L \dot{b}_f\delta p\,\mathrm{d}x_1 + c_f\int_0^L b_{f0}\dot{p}\delta p\,\mathrm{d}x_1\right] \quad (32)$$

In formulation of equation (32), the normal flow rate V_n^* is substituted by $-v_n$, the approach of integral by parts is employed, and the derivative $(b_{f0})_{,1}$ is neglected. Equation (30) can be imposed in the variational principle also. Noting that $T_2 = P_2^*$ and $b_f = 2u_2$, the second integral from the end of equation (17) has the following variational form:

$$\delta\Pi_\sigma = \delta\int_{S_\sigma} P_i^* u_i\,\mathrm{d}S = \int_0^L T_2\,\delta u_2\,\mathrm{d}x_1 = \int_0^L\left(\lambda_f p - E_f\frac{2u_2 - b_{f0}}{b_{f0}}\right)\delta u_2\,\mathrm{d}x_1 \quad (33)$$

FINITE ELEMENT DISCRETIZATION

Equations (17) and (18) can be converted into two sets of algebraic equations by using finite element method. In this section, the bold symbols denote vectors, columns or matrices. Let $\mathbf{u}$, $\boldsymbol{\varepsilon}$ and p be the displacement, strain and pore pressure respectively and $\hat{\mathbf{u}}$ and $\hat{\mathbf{p}}$ be the columns of the nodal displacements and the nodal pore pressures of an element respectively. Then, the expressions for $\mathbf{u}$, $\boldsymbol{\varepsilon}$, p, ε_{ij} and $\mathbf{grad}(p)$ in the element can take the following forms:

$$\mathbf{u} = \mathbf{N}_u\hat{\mathbf{u}} \quad (34a)$$

$$\boldsymbol{\varepsilon} = \mathbf{B}\hat{\mathbf{u}} \quad (34b)$$

$$p = \mathbf{N}_p\hat{\mathbf{p}} \quad (34c)$$

$$\varepsilon_{ii} = \mathrm{div}(\mathbf{u}) = \mathbf{d}\hat{\mathbf{u}} \quad (34d)$$

$$\mathbf{grad}(p) = \mathbf{g}\hat{\mathbf{p}} \quad (34e)$$

where $\mathbf{N}_u$ and $\mathbf{N}_p$ are the shape functions for displacement and pore pressure, respectively, within the element. Symbol div is the divergence operator and symbol **grad** is the gradient operator. The finite element discretization for equations (17) and (18) gives the following result:

$$\delta\Phi = \sum_e \delta\hat{\mathbf{u}}^{\mathrm{T}}\left[\int_{V_e}\mathbf{B}^{\mathrm{T}}\mathbf{D}\mathbf{B}\,\mathrm{d}V\,\hat{\mathbf{u}} - \lambda\int_{V_e}\mathbf{d}^{\mathrm{T}}\mathbf{N}_p\,\mathrm{d}V\hat{\mathbf{p}}\right]$$
$$-\sum_e \delta\hat{\mathbf{p}}^{\mathrm{T}}\left[\frac{K}{a_0}\int_{V_e}\mathbf{g}^{\mathrm{T}}\mathbf{g}\,\mathrm{d}V\,\hat{\mathbf{p}} + c\int_{V_e}\mathbf{N}_p^{\mathrm{T}}\mathbf{N}_p\,\mathrm{d}V\,\hat{\mathbf{p}} + \lambda\int_{V_e}\mathbf{N}_p^{\mathrm{T}}\mathbf{d}\,\mathrm{d}V\,\hat{\mathbf{u}}\right]$$
$$-\sum_e \delta\hat{\mathbf{p}}^{\mathrm{T}}\left[\frac{\lambda}{a_0}\left(a_{-2}\int_{V_e}\mathbf{N}_p^{\mathrm{T}}\mathbf{d}\,\mathrm{d}V\hat{\mathbf{u}}_{-2} + a_{-1}\int_{V_e}\mathbf{N}_p^{\mathrm{T}}\mathbf{d}\,\mathrm{d}V\hat{\mathbf{u}}_{-1}\right)\right]$$
$$-\sum_e \delta\hat{\mathbf{p}}^{\mathrm{T}}\left[\frac{c}{a_0}\left(a_{-2}\int_{V_e}\mathbf{N}_p^{\mathrm{T}}\mathbf{N}_p\,\mathrm{d}V\hat{\mathbf{p}}_{-2} + a_{-1}\int_{V_e}\mathbf{N}_p^{\mathrm{T}}\mathbf{N}_p\,\mathrm{d}V\hat{\mathbf{p}}_{-1}\right)\right]$$
$$-\sum_e \delta\hat{\mathbf{u}}^{\mathrm{T}}\int_{S_\sigma^e}\mathbf{N}_u^{\mathrm{T}}\mathbf{P}^*\,\mathrm{d}S - \sum_e\delta\hat{\mathbf{p}}^{\mathrm{T}}\frac{1}{a_0}\int_{S_v^e}\mathbf{N}_p^{\mathrm{T}}V_n^*\,\mathrm{d}S = 0 \quad (35)$$

where the symbol $\sum_e$ means the summation over all the elements in the domain V if volume integration is taken, or the summation over the elements which share the boundary S_σ or S_v of the domain V if surface integration is taken. V_e is the volume of the element, S_σ^e is a part of the element boundary where the traction is prescribed, S_v^e is a part of the element boundary where the flow rate is prescribed. $\mathbf{D}$ is the elasticity matrix for the solid skeleton. Through the procedure of matrix assemblage, equation (35) becomes

$$\delta\Phi = \delta\hat{\mathbf{U}}^{\mathrm{T}}[\mathbf{K}\hat{\mathbf{U}} - \mathbf{L}\hat{\mathbf{P}}] - \delta\hat{\mathbf{P}}^{\mathrm{T}}\left[\frac{1}{a_0}\mathbf{G}\hat{\mathbf{P}} + \mathbf{C}\hat{\mathbf{P}} + \mathbf{L}^{\mathrm{T}}\hat{\mathbf{U}}\right] - \delta\hat{\mathbf{P}}^{\mathrm{T}}\left[\frac{1}{a_0}(a_{-2}\mathbf{L}^{\mathrm{T}}\hat{\mathbf{U}}_{-2} + a_{-1}\mathbf{L}^{\mathrm{T}}\hat{\mathbf{U}}_{-1} + a_{-2}\mathbf{C}\hat{\mathbf{P}}_{-2} + a_{-1}\mathbf{C}\hat{\mathbf{P}}_{-1}\right] - \delta\hat{\mathbf{U}}^{\mathrm{T}}\mathbf{F} - \frac{1}{a_0}\delta\hat{\mathbf{P}}^{\mathrm{T}}\mathbf{Q} = 0 \tag{36}$$

where

$$\mathbf{K} = \sum_e \int_{V_e} \mathbf{B}^{\mathrm{T}}\mathbf{D}\mathbf{B}\,\mathrm{d}V \tag{37a}$$

$$\mathbf{L} = \sum_e \lambda \int_{V_e} \mathbf{d}^{\mathrm{T}}\mathbf{N}_{\mathrm{p}}\,\mathrm{d}V \tag{37b}$$

$$\mathbf{G} = \sum_e K \int_{V_e} \mathbf{g}^{\mathrm{T}}\mathbf{g}\,\mathrm{d}V \tag{37c}$$

$$\mathbf{C} = \sum_e c \int_{V_e} \mathbf{N}_{\mathrm{p}}^{\mathrm{T}}\mathbf{N}_{\mathrm{p}}\,\mathrm{d}V \tag{37d}$$

$$\mathbf{F} = \sum_e \int_{S_\sigma^e} \mathbf{N}_u^{\mathrm{T}}\mathbf{P}^*\,\mathrm{d}S \tag{37e}$$

$$\mathbf{Q} = \sum_e \int_{S_v^e} \mathbf{N}_{\mathrm{p}}^{\mathrm{T}}V_n^*\,\mathrm{d}S \tag{37f}$$

$\hat{\mathbf{U}}$ is the global column of nodal displacements and $\hat{\mathbf{P}}$ is the global column of nodal pressures. In equations (37a)–(37f), symbol $\sum_e$ denotes the assemblage procedure for matrices or columns. Equation (36) is valid for arbitrary values of the variations of $\delta\hat{\mathbf{U}}$ and $\delta\hat{\mathbf{P}}$ and can hence leads to

$$\mathbf{K}\hat{\mathbf{U}} - \mathbf{L}\hat{\mathbf{P}} = \mathbf{F} \tag{38}$$

$$-\frac{1}{a_0}\mathbf{L}^{\mathrm{T}}(a_0\hat{\mathbf{U}} + a_{-1}\hat{\mathbf{U}}_{-1} + a_{-2}\hat{\mathbf{U}}_{-2}) - \frac{1}{a_0}\mathbf{G}\hat{\mathbf{P}} - \frac{1}{a_0}\mathbf{C}(a_0\hat{\mathbf{P}} + a_{-1}\hat{\mathbf{P}}_{-1} + a_{-2}\hat{\mathbf{P}}_{-2}) = \frac{1}{a_0}\mathbf{Q} \tag{39}$$

Using equation (15) and eliminating the coefficient a_0 in both sides, equation (39) can return to the form including time derivatives of the field variables, i.e.

$$-\mathbf{L}^{\mathrm{T}}\dot{\hat{\mathbf{U}}} - \mathbf{G}\hat{\mathbf{P}} - \mathbf{L}\dot{\hat{\mathbf{P}}} = \mathbf{Q} \tag{40}$$

Equation (38) and (40) are the same as the finite element equations obtained by Huang *et al.*[12] For convenience in computation, the known terms in equation (39) can be moved to the right hand

side of the equation. Therefore, we obtain the following preference:

$$-\mathbf{L}^{\mathrm{T}}\hat{\mathbf{U}}-\left(\frac{1}{a_0}\mathbf{G}+\mathbf{C}\right)\hat{\mathbf{P}}=\frac{1}{a_0}\left[\mathbf{Q}+\mathbf{L}^{\mathrm{T}}(a_{-1}\hat{\mathbf{U}}_{-1}+a_{-2}\hat{\mathbf{U}}_{-2})+\mathbf{C}(a_{-1}\hat{\mathbf{P}}_{-1}+a_{-2}\hat{\mathbf{P}}_{-2})\right] \tag{41}$$

Equations (38) and (41) are the global finite element equations for the porous media. It can be seen that both the equations include the columns of nodal displacements and nodal pressures. Hence, the two equations are fully coupled.

The conductive fracture can be partitioned into one-dimensional elements. Pertinent shape functions for displacement and pore pressure can be defined within elements. For convenience in elaborating this finite element method, it is assumed that each element has two nodes at its ends and the shape functions for displacement and pressure in the element are linear functions of coordinate x_1. Thus, the first integral in equation (23) can be written as

$$\int_0^{L(t)} b_{\mathrm{f}}p_{,1}\delta p_{,1}\mathrm{d}x_1=\sum_{i=1}^{n}\left[\delta p^{(i-1)}\,\delta p^{(i)}\right]\frac{\bar{b}_{\mathrm{f}}^{(i)}}{l^{(i)}}\begin{bmatrix}1 & -1\\ -1 & 1\end{bmatrix}\begin{Bmatrix}p^{(i-1)}\\ p^{(i)}\end{Bmatrix} \tag{42}$$

where $l^{(i)}$ is the length of the ith element, $\bar{b}_{\mathrm{f}}^{(i)}$ is the average value of the width of the element, the superscripts (i) and $(i-1)$ denote the two nodes of the ith element and n is the total number of the elements of the conductive fracture. The second integral in equation (23) can be written as

$$\int_0^{L(t)}\dot{b}_{\mathrm{f}}\delta p\,\mathrm{d}x_1=\sum_{i=1}^{n}l^{(i)}\left[\delta p^{(i-1)}\delta p^{(i)}\right]\begin{bmatrix}1/3 & 1/6\\ 1/6 & 1/3\end{bmatrix}\begin{Bmatrix}a_0(b_{\mathrm{f}})^{(i-1)}+a_{-1}(b_{\mathrm{f}})_{-1}^{(i-1)}+a_{-2}(b_{\mathrm{f}})_{-2}^{(i-1)}\\ a_0(b_{\mathrm{f}})^{(i)}+a_{-1}(b_{\mathrm{f}})_{-1}^{(i)}+a_{-2}(b_{\mathrm{f}})_{-2}^{(i)}\end{Bmatrix} \tag{43}$$

and the third integral in equation (23) becomes

$$\int_0^{L(t)}b_{\mathrm{f}}\dot{p}\delta p\,\mathrm{d}x_1=\sum_{i=1}^{n}\bar{b}^{(i)}{}_{\mathrm{f}}l^{(i)}\left[\delta p^{(i-1)}\delta p^{(i)}\right]\begin{bmatrix}1/3 & 1/6\\ 1/6 & 1/3\end{bmatrix}\begin{Bmatrix}a_0p^{(i-1)}+a_{-1}p_{-1}^{(i-1)}+a_{-2}p_{-2}^{(i-1)}\\ a_0p^{(i)}+a_{-1}p_{-1}^{(i)}+a_{-2}p_{-2}^{(i)}\end{Bmatrix} \tag{44}$$

Equations (42)–(44) are in a format ready for assembling into the global finite element equation (41). The three integrals in equation (32) can also have the same expressions as equations (42)–(44), but the average crack width in an interval $\bar{b}_{\mathrm{f}}^{(i)}$ should be replaced by $\bar{b}_{\mathrm{f}0}^{(i)}$.

With the use of the approach in analysing equation (23), equation (33) can be written as

$$\begin{aligned}\delta\Pi_\sigma=\int_0^{L}T_2\delta u_2\,\mathrm{d}x_1=\sum_{i=1}^{n}\left[\delta u_2^{(i-1)}\delta u_2^{(i)}\right]\Bigg(&\lambda_{\mathrm{f}}l^{(i)}\begin{bmatrix}1/3 & 1/6\\ 1/6 & 1/3\end{bmatrix}\begin{Bmatrix}p^{(i-1)}\\ p^{(i)}\end{Bmatrix}\\ &-\frac{2E_{\mathrm{f}}}{\bar{b}_{\mathrm{f}0}^{(i)}}l^{(i)}\begin{bmatrix}1/3 & 1/6\\ 1/6 & 1/3\end{bmatrix}\begin{Bmatrix}u_2^{(i-1)}\\ u_2^{(i)}\end{Bmatrix}+E_{\mathrm{f}}l^{(i)}\begin{Bmatrix}1/2\\ 1/2\end{Bmatrix}\Bigg)\end{aligned} \tag{45}$$

Equation (45) is also in a format ready for assembling into the global finite element equation (38).

In fact, the elements in the reservoir adjacent to the crack surface and the elements of the conductive fracture can share the same nodes. Hence, each one-dimensional elements of the conductive fracture is also a side of an element adjacent to the crack surface. As will be seen in our example problem, four node isoparametric elements for plane strain will be used. Hence, field quantities vary linearly on the boundary of the elements. While the shape functions of the one-dimensional elements are also linear functions of coordinate x_1. Thus, the field quantities in the reservoir and in the conductive fracture are continuous across the crack surface.

COMPUTATIONAL SCHEMES

As afore-mentioned, the poroelastic medium is modelled as a plane strain problem. Hereafter, the Latin subscripts denoting the co-ordinates will be replaced by Greek subscripts with the value 1 or 2. In our finite element method, four node quadrilateral parametric elements are employed in the domain. Within the element which does not include crack tip, displacement components take the following regular form:

$$u_\alpha = u_\alpha^I(1-\xi)\eta + u_\alpha^J(1-\xi)(1-\eta) + u_\alpha^K(1-\eta)\xi + u_\alpha^L\eta\xi \tag{46}$$

with the transformation

$$x_\alpha = x_\alpha^I(1-\xi)\eta + x_\alpha^J(1-\xi)(1-\eta) + x_\alpha^K(1-\eta)\xi + x_\alpha^L\eta\xi \tag{47}$$

where I, J, K and L are four node numbers of the element, ξ and η are isoparametric co-ordinates. Transformation (47) maps the quadrilateral $IJKL$ on the x_1–x_2 plane onto a unit square $IJKL$ on ξ–η plane with the corners $I(0, 1)$, $J(0, 0)$, $K(1, 0)$ and $L(1, 1)$. However, as a result of $r^{-1/2}$ singularity, where r is the radial distance of a point in the medium measured from the crack tip, in stress and strain, the displacement components in an element adjacent to the crack tip take a singular form suggested by Rice and Tracey:[14]

$$u_\alpha = u_\alpha^I(1-\xi^{1/2})\eta + u_\alpha^J(1-\xi^{1/2})(1-\eta) + u_\alpha^K(1-\eta)\xi^{1/2} + u_\alpha^L\eta\xi^{1/2} \tag{48}$$

with $u_\alpha^I = u_\alpha^J = u_\alpha^{IJ}$. In fact, these elements are triangular elements, as shown in Figure 2, degenerated from quadrilaterals $IJKL$ with the nodes I and J connected at the crack tip. Transformation (47) still maps the triangular element onto the unit square $IJKL$ on ξ–η plane. Rice and Tracey proved that the displacement components expressed by equation (48) are proportional to $r^{1/2}$ within the element, resulting in an $r^{-1/2}$ singularity in stress and strain near the crack tip. The interpolation formula for the pore pressure takes a regular bilinear form, the same as equation (46) with the displacement components u_α replaced by pore pressure p, for all the elements in the finite region.

In the analysis of transient problems, if the infinite domain is simply replaced by a sufficiently large finite domain, finite element solution is accurate only for small time. With the increase in time the loading on the internal boundary, such as the pore pressure on the internal crack surface, will disturb the outer boundary of the finite domain after all, no matter how large the finite domain is. To overcome this disadvantage, the infinite elements based on the nodal displacements and the pore pressure, respectively, on the outer boundary of the finite domain are employed in the region outside the finite domain, as shown in Figure 2.

The infinite element associated with pore pressure was presented by Li.[4] He suggested that the pore pressure in the region outside the finite domain take the following form:

$$p = N(\xi, t)\bar{p} = \frac{\mathrm{Ei}(e^{2\xi}/16t_\mathrm{D})}{\mathrm{Ei}(e^{2\bar{\xi}}/16t_\mathrm{D})}\bar{p} \tag{49}$$

where Ei is the exponential function, ξ is one of the co-ordinate parameters in an elliptical co-ordinate system and defined by

$$\begin{aligned} x_1 &= L\cosh\xi\cos\eta \\ x_2 &= L\sinh\xi\sin\eta \end{aligned} \tag{50}$$

$\bar{\xi}$ is the value of ξ on the outer boundary of the finite domain, $\bar{p}$ is the value of p on the outer boundary of the finite domain, t_D is the dimensionless time defined by

$$t_D = \frac{\kappa t}{L^2} \tag{51}$$

where κ is the diffusion coefficient defined by $\kappa = K/c$.

The shape function with $1/R$ type decay for the displacements in the infinite elements presented by Lynn and Hadid[15] is used in the computation. If each infinite element has two nodes defined on the outer boundary of the finite domain, the displacement components in the infinite element can be expressed by

$$u_\alpha = \frac{\bar{R}}{R}\left(\frac{\theta^{(i)} - \theta}{\theta^{(i)} - \theta^{(i-1)}}\, u_\alpha^{(i-1)} + \frac{\theta - \theta^{(i-1)}}{\theta^{(i)} - \theta^{(i-1)}}\, u_\alpha^{(i)}\right) \tag{52}$$

where R and θ are the polar radius and polar angle, respectively, for material points in the infinite elements with the origin of the polar co-ordinate system at the crack center as shown in Figure 2. $\bar{R}$ is the polar radius of the points on the outer boundary of the finite domain. Superscripts $(i-1)$ and (i) stand for the two nodes of the infinite element on the outer boundary. The quantities with the superscripts are defined at node $i-1$ or node i. It can be proved easily that $1/R$ type decay is in accordance with the first order asymptotic solution of displacements for the classical problem in linear elastic fracture mechanics, namely, a crack in an infinite medium with a traction on the crack surface.

The stress intensity factor K_I is evaluated from the nodal displacements in front of the crack tip. According to the Williams formula,[16] the horizontal displacement of a point on the extension of the crack relative to the crack tip can be expressed by

$$u_1(x_1, 0) - u_1[L(t), 0] = \frac{K_1}{G}\left(\frac{r}{2\pi}\right)^{1/2}(1 - 2v) \quad \text{for } r \to 0 \tag{53}$$

where G is the shear modulus of the medium, v is the Poisson's ratio of the medium and π is the circle ratio, $r = x_1 - L(t) > 0$. Consequently, the stress intensity factor can be written as

$$K_I = \frac{G}{1 - 2v}\{u_1(x_1, 0) - u_1[L(t), 0]\}\left(\frac{2\pi}{r}\right)^{1/2} \quad \text{for } r \to 0 \tag{54}$$

Hence, the stress intensity factor can be calculated from the displacements at the nodal points on the extension of the crack with the use of equation (54). The value of K_I at $r = 0$ can be determined by extrapolation of the K_I versus r curve back to the crack tip. This method was presented by Chen *et al.*[17]. Since singular elements are used near the crack tip, the displacements obtained by using our finite element method are accurate. This method is used to calculate a stress intensity factor for the case of a crack in an infinite medium with a uniformly distributed traction applied on the crack surface. The numerical result of K_I is found to be very close to the theoretical value.

A moving and relaying elements technique is adopted for conductive fracture growth. The finite element mesh of an example problem to be studied in the next section is shown in Figure 2. The grey area at the bottom of this figure is the moving elements area. The procedure of element translation and re-arrangement is shown in Figure 3, where the moving elements areas are shaded. The moving elements translate with the same speed as the tip of the growing crack and

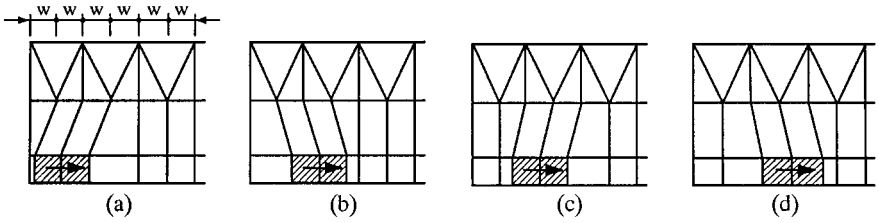

Figure 3. Elements re-meshing in the vicinity of the moving elements area

maintain at fixed relative positions with respect to the crack tip. Figure 3(a) indicates the initial location of the moving elements. In the translating procedure of the moving elements as indicated from Figure 3(a) to 3(b), the elements adjacent to the moving elements area only change their shapes. When the moving elements move to the position as shown in Figure 3(b), elements relaying will be taken. Figure 3(c) denotes the mesh in the vicinity of the moving elements after the relaying. Figure 3(d) indicates that the moving elements continue translating after element relaying. In the example problem, elements relaying is taken when the crack length reaches $(n + 0{\cdot}5)w$, where n is a positive integer and w is an element size in the vicinity of the moving elements area as shown in Figure 3(a). With this technique, the moving elements can keep up with the crack growth until the terminal crack length 100·0 ft is reached.

In each step of crack growth, the nodal points in the moving elements area will arrive at new positions. The values of the field quantities in previous steps at the new positions need to be determined to calculate the column on the right hand side of the global finite element equation, equation (41). An isoparametric interpolation is employed for determination of these values. First of all, one need to determine the elements which include the nodes at the new positions. Let I, J, K and L denote the four corners of the element in a previous step and $\overline{IJ}$ be a vector with the direction from I to J. Hence, the four sides of the element can be expressed in vector forms as $\overline{IJ}$, $\overline{JK}$, $\overline{KL}$ and $\overline{LI}$. If the node at the new position is denoted by A, one also has vectors $\overline{IA}$, $\overline{JA}$, $\overline{KA}$ and $\overline{LA}$. Now, node A is located within element $IJKL$ if and only if the four cross products

$$\overline{IJ} \times \overline{IA},\ \overline{JK} \times \overline{JA},\ \overline{KL} \times \overline{KA},\ \overline{LI} \times \overline{LA}$$

are all in the positive direction of x_3, where x_3 is a co-ordinate axis perpendicular to the $x_1 - x_2$ plane and the x_1-, x_2- and x_3-axes form a right-hand coordinate system. If node A is judged to be within element $IJKL$, the local isoparametric co-ordinates (ξ, η) can be determined by equation (47) with the coordinates x_α substituted by x_α^A. Since the shape functions in equation (47) are bilinear functions of ξ and η, four sets of solutions for ξ and η can be obtained. Only the solution satisfying the conditions $0 < \xi < 1$ and $0 < \eta < 1$ is reasonable. Then the field quantities at point A can be determined by equation (46) for regular elements or (48) for singular elements. This is so-called isoparametric interpolation.

According to equation (23) and (32) with the use of the variational principle, equations (17) and (18), if the pressure at the well-bore is prescribed, the flow rate q_w at the well-bore can be obtained by

$$0{\cdot}25 q_w = a_0 \frac{\partial \Phi}{\partial p_w} \tag{55}$$

In fact, this is the difference of both sides of the algebraic equation in the global finite element equation (41) corresponding to the node number at the well-bore. This is the best way to determine the flow rate q_w as discussed in Reference 4.

To save CPU time and to facilitate computer program design, the two sets of algebraic equations (38) and (41) are solved separately. Since the two sets of equations are coupled, a nested iteration between them proceeds until a pertinent tolerance of errors is reached. Another iterative loop is needed for correction of the applied pressure at the well-bore in order to maintain the fracture criterion, equation (19).

AN EXAMPLE

Consider a fully penetrating vertical fracture with the well located at its mid-point. The following material and geometrical constants for a typical sandstone oil formation and a sand-formed finite conductivity fracture are employed in our computation:

$K = 0{\cdot}08639\ \mathrm{m^2/MPa/day}$ ($4{\cdot}453 \times 10^{-5}\ \mathrm{ft^2/psf/day}$),[†] $G = 6\ \mathrm{GPa}$ ($1{\cdot}253 \times 10^8\ \mathrm{psf}$)
$\nu = 0{\cdot}15$, $\lambda = 0{\cdot}6372$, $c = 0{\cdot}071 \times 10^{-3}\ \mathrm{MPa^{-1}}$ ($0{\cdot}34 \times 10^{-8}\ \mathrm{psf^{-1}}$), $\phi = 0{\cdot}1$
$K_{IC} = 10{\cdot}05\ \mathrm{MPa \cdot m^{1/2}}$ ($38{\cdot}0 \times 10^4\ \mathrm{psf \cdot ft^{1/2}}$)
$E_f = 7{\cdot}5\ \mathrm{GPa}$ ($1{\cdot}566 \times 10^8\ \mathrm{psf}$), $\lambda_f = 0{\cdot}5012$, $c_f = 0{\cdot}071 \times 10^{-3}\ \mathrm{MPa^{-1}}$ ($0{\cdot}34 \times 10^{-8}\ \mathrm{psf^{-1}}$)
$L = 30{\cdot}48\ \mathrm{m}$ (100 ft)
$K_f = 1000 \times K = 86{\cdot}39\ \mathrm{m^2/MPa/day}$ ($0{\cdot}04453\ \mathrm{ft^2/psf/day}$), $\phi_f = 0{\cdot}15$ for case 1 and
$K_f = 10\,000 \times K = 863{\cdot}9\ \mathrm{m^2/MPa/day}$ ($0{\cdot}4453\ \mathrm{ft^2/psf/day}$), $\phi_f = 0{\cdot}25$ for case 2

These values of the material constants were used in References 5 and 12. As mentioned previously, the five material constants G, ν, ν_u, B and K can completely define a poroelastic medium. They can be measured experimentally. Constants λ, c, λ_f and c_f can be determined by equations (9) and (10).

The *in-situ* stress components in the formation are $\sigma_{11}^{\infty} = -2000\ \mathrm{psi}$[‡] and $\sigma_{22}^{\infty} = -1500\ \mathrm{psi}$ (compression), and the initial pore pressure in the formation is $p_0 = 800\ \mathrm{psi}$. An initial crack with half length of $L_0 = 6{\cdot}0$ ft adjacent to the well-bore is generated *in priori*. Time increment method is utilized in our computation. When the pressure applied to the well exceeds the magnitude of the *in-situ* stress σ_{22}^{∞} by Δp, the crack will open. In the initial time increment, it is assumed that there is no sand in the crack and the applied pressure is uniformly distributed on the crack surface. The applied pressure increases until the stress intensity factor at the crack tip reaches the fracture toughness K_{IC}. Afterwards, the crack grows gradually with sand filled in it simultaneously. The crack grows at a constant speed of 100·0 ft/day. The increment of the semi-crack length is $\Delta L = 0{\cdot}5$ ft. Correspondingly, the time increment is $\Delta t = 0{\cdot}005$ day. Two cases for different crack-filling material, case 1 for lower permeability material and case 2 for higher permeability material, are considered in the computation.

Since the initial pore pressure and the *in-situ* stresses in the medium are nonzero, the problem of the conductive fracture growing can be regarded as a superposition of two sub-problems as shown in Figure 4(a). The first sub-problem has the solution of a uniform stress field with $\sigma_{11} = -2000\ \mathrm{psi}$, $\sigma_{22} = -1500\ \mathrm{psi}$ and $\sigma_{12} = 0$, and a uniform pore pressure field with

[†] 1 ft = 0·3048 m; 1 psf = 47·88 Pa
[‡] 1 psi = 6·895 kPa

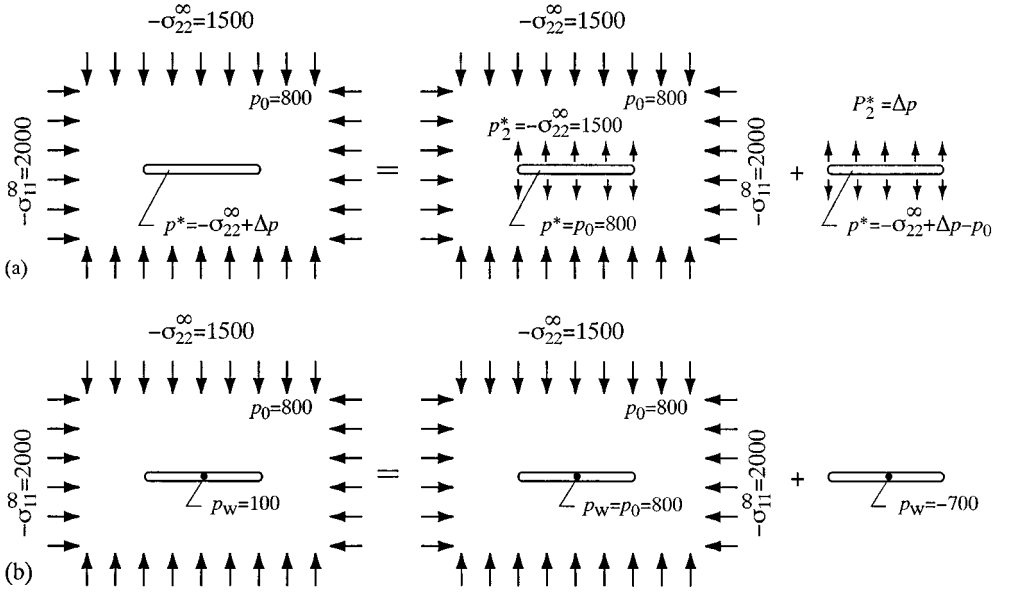

Figure 4. Superposition method for the example problem: (a) An applied pressure $p^* = -\sigma_{22}^{\infty} + \Delta p$ acts in the initial crack; (b) the applied pressure at the well-bore p_w drops to 100 psi when the conductive crack is generated

$p = 800$ psi. This field generates neither stress intensity factor nor fluid flow in the medium, and can be regarded to be undeformed. In the second sub-problem, the initial stress and the initial pore pressure are zero in the medium. The traction on the crack surface is $P^* = \Delta p$. The pore pressure in the crack is $p^* = -\sigma_{22}^{\infty} + \Delta p - p_0$. The second sub-problem can be analysed by means of the finite element method based on the variational principle, equations (17) and (18). It has to be noted that the traction on the crack surface is not equal to the pore pressure any longer and there is always a difference of $-\sigma_{22}^{\infty} - p_0$ between them.

When the conductive fracture reaches the terminal length $L = 100$ ft, the applied pressure at the well-bore drops to 100 psi and the crack growth is arrested. A sustained stationary fracture is then formed. This problem can also be divided into two sub-problems as shown in Figure 4(b). Analysis of the transient behavior of the deformation and the pore pressure for the second sub-problem can be continued from the end of the second sub-problem in Figure 4(a) with the applied pressure $p_w = -700$ psi applied at the well-bore. The real solution for the problem of the sustained stationary conductive crack can be obtained by superposition of these two sub-problems.

Numerical results for the problem of the growing crack are shown in Figures 5–9. It is found that the curves shown in Figures 5–7 oscillate with the increasing semi-crack length. However, if these curves are smoothed, one can find the tendency that the injection rate q_w drops rapidly in the first time step because the empty crack changes to a sand-filled conductive crack. Later on it decreases gradually since the applied pressure drops with the increasing crack length. It reaches a minimum value in the interval of $L(t) = 10$–20 ft as shown in Figures 5(a) and 5(b). The curves of the applied pressure at the well-bore versus the semi-crack length are shown in Figures 6(a) and 6(b).

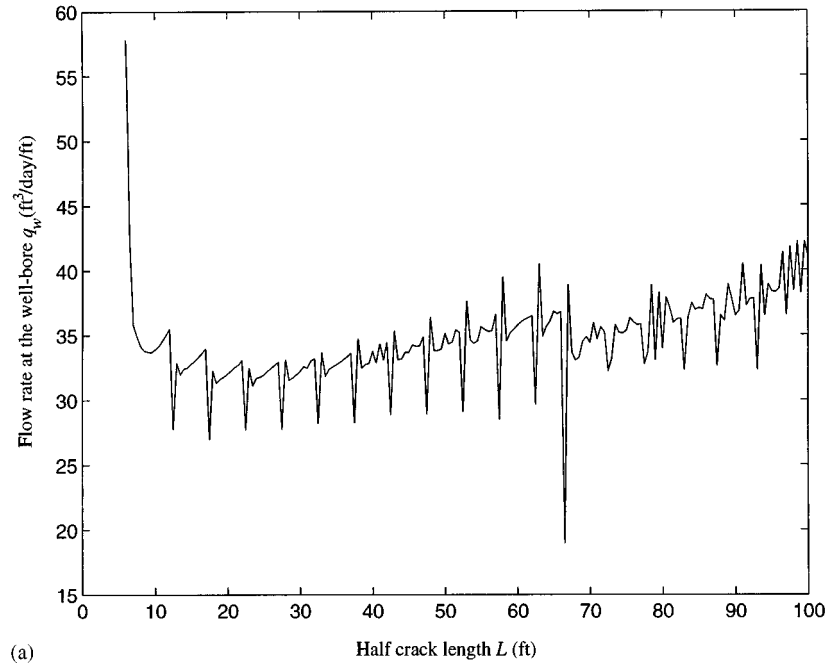

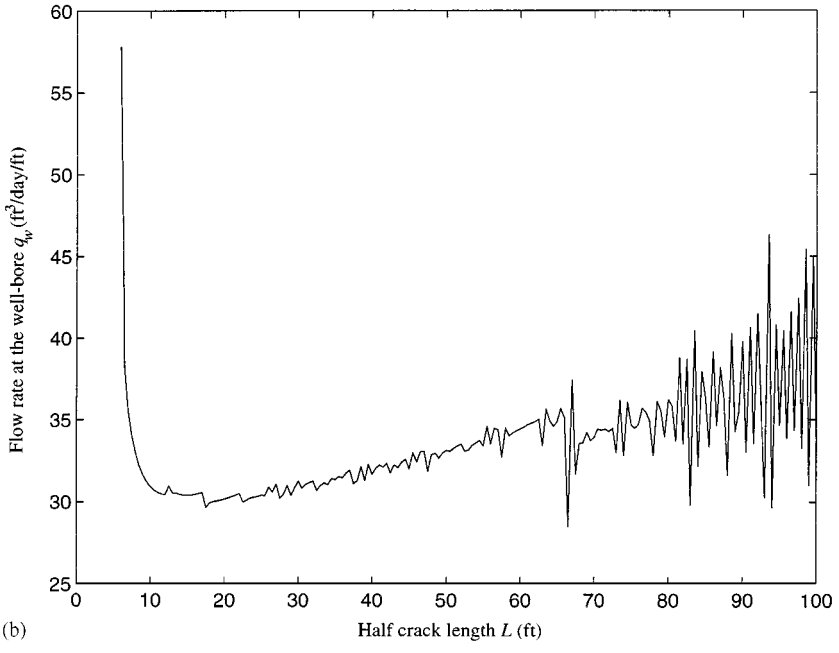

Figure 5. The curve of the flow rate at the well-bore vs. transient half crack length (a) ($K_f = 1000\,K$, $\phi_f = 0{\cdot}15$); (b) ($K_f = 10\,000\,K$, $\phi_f = 0{\cdot}25$)

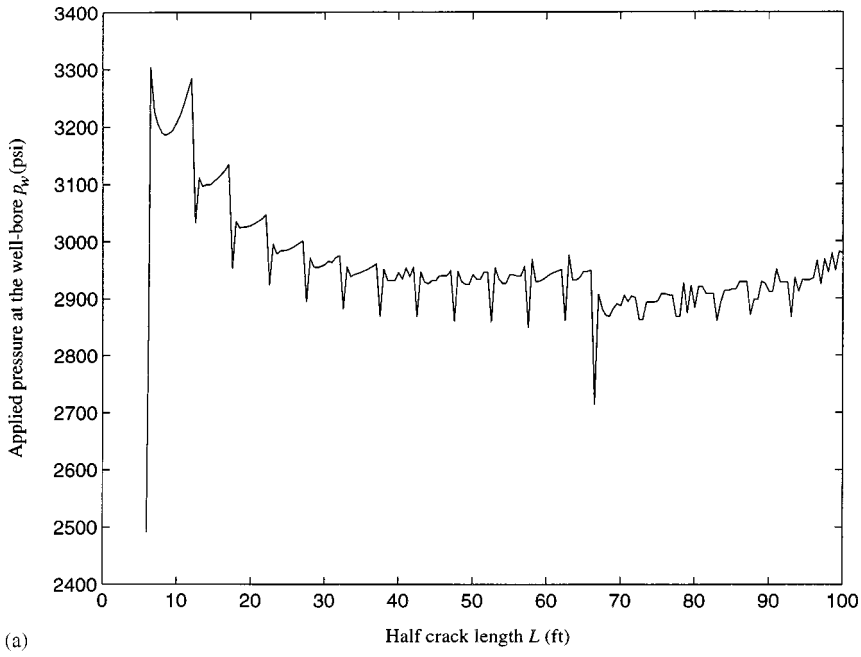

(a)

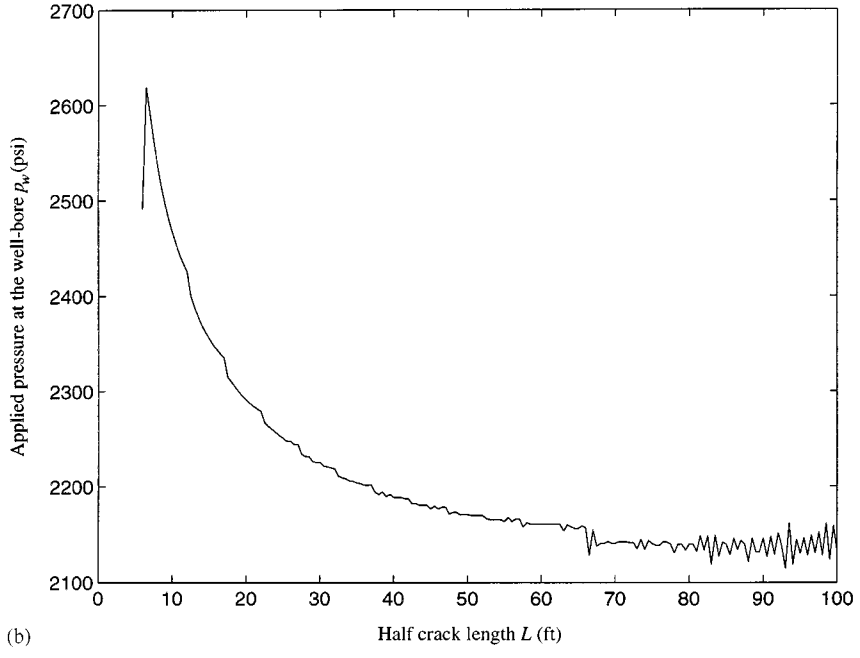

(b)

Figure 6. The curve of the applied pressure at the well-bore vs. transient half crack length (a) ($K_f = 1000\,K$, $\phi_f = 0{\cdot}15$); (b) ($K_f = 10\,000\,K$, $\phi_f = 0{\cdot}25$)

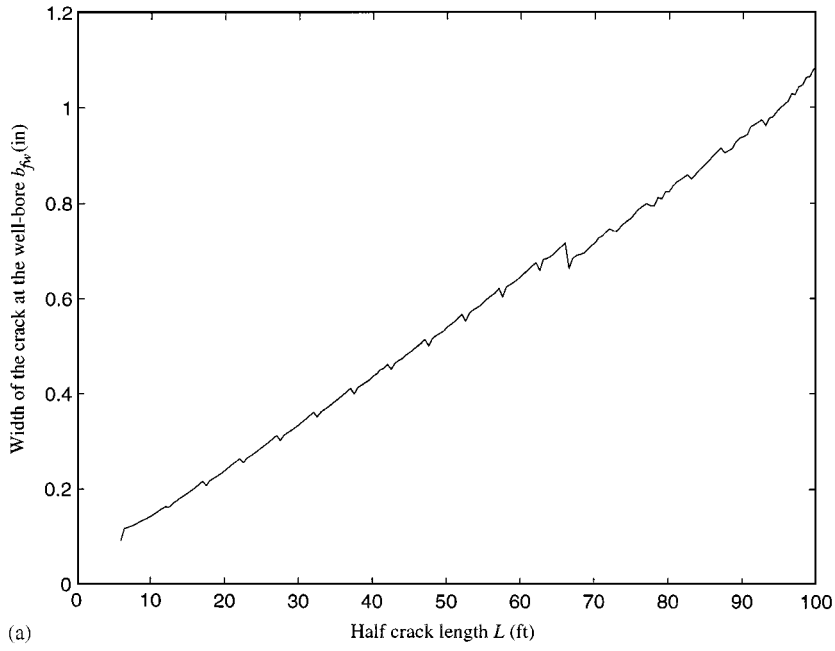

(a)

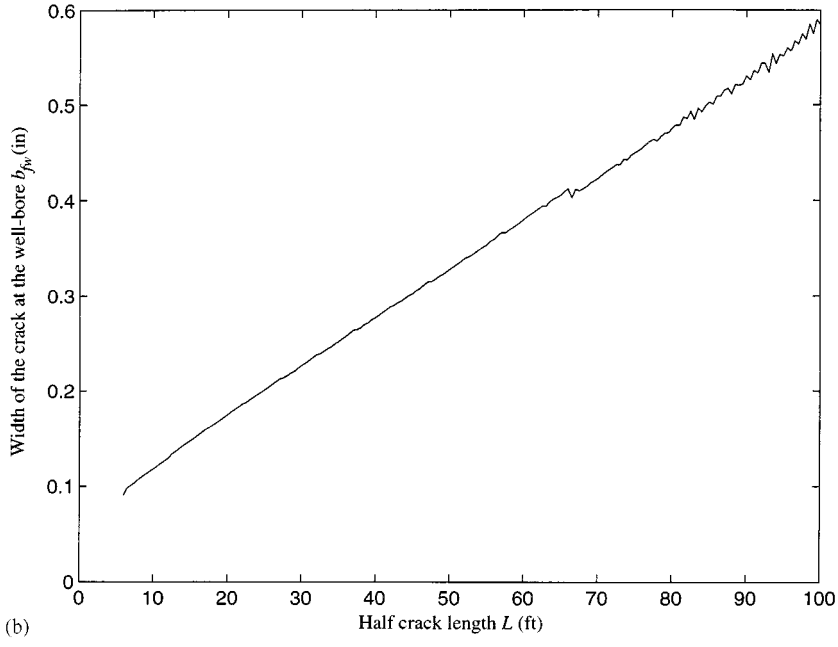

(b)

Figure 7. The curve of the width of the crack at the well-bore vs. transient half crack length (a) ($K_f = 1000\ K$, $\phi_f = 0{\cdot}15$); (b) ($K_f = 10\,000\ K$, $\phi_f = 0{\cdot}25$)

It is found that the applied pressure increases with the crack length in the first time step since it must overcome the resistance for crack growth resulting from the fracture toughness. On the other hand, in this step the empty crack changes to a sand-filled conductive crack. Hence, larger applied pressure is necessary to force the injected fluid to flow into the fracture and diffuse into the formation. The applied pressure at the well-bore decreases gradually thereafter since the crack length becomes longer and even less applied pressure can maintain the stress intensity factor K_I at the level K_{IC}. The width of the crack at the well-bore b_{fw}, sometimes called the crack mouth opening displacement, increases monotonically and almost linearly with the crack length as shown in Figures 7(a) and 7(b).

The oscillation of these curves can be attributed to the difference of the speeds between crack propagation and the seepage flow in the crack. When the speed of the seepage flow is lower than that of the crack propagation, there exists a local low pressure region near the crack tip. In this period, distribution of the transient pore pressure and its values in the fracture essentially do not vary with time because they still can maintain K_I at the level K_{IC}. However, the local low pressure region near the crack tip raises the magnitude of the pressure gradient and increases the permeating velocity near the crack tip. The seepage flow may catch the crack tip sometime later. Consequently, the pore pressure in the local low pressure region generated in the previous steps can increase or even exceed its regular value. The increase in pressure in this region will raise the value of the stress intensity factors K_I effectively. Thus, in order to maintain the fracture criterion, equation (19), the applied pressure at the well-bore will decrease so that the pressure in the crack can be lowered. The magnitude of the pressure gradient and the permeating velocity in the crack then decrease and the local low pressure region near the crack tip appears again. This procedure can be repeated continuously. Hence, oscillation of the applied pressure p_{w} occurs. The oscillation in p_{w} also leads to the oscillation in the injection rate q_{w} and the crack mouth opening displacement at the well-bore b_{fw}. Generally speaking, the amplitude of the oscillation increases when the crack gets longer because the influence of p_{w} on the pressure near the crack tip becomes weaker. Since the permeability of the crack in case 2 is higher than that in case 1, pressure diffuses into the crack in case 2 more easily than in case 1. Hence, the curves in case 2 oscillates less drastically than in case 1 in general. It is seen that although the curves in the two cases have the same tendency, the respective shapes in the two cases are obviously different.

Figures 8 and 9 show the transient pore pressure fields by isobars in the reservoir near the fracture at the length of the growing crack $L(t) = 47{\cdot}5$ ft and $L(t) = 100$ ft respectively. The isobars in these figures appear reasonably distributed. For a same material point in the reservoir, the pore pressure in case 1 is larger than that in case 2. The reason is that because the permeability of the crack-filling material in case 1 is lower than that in case 2, a larger magnitude of pressure gradient is needed for case 1 to keep the fluid injecting into the fracture. Correspondingly, a larger applied pressure at the well-bore p_{w} is needed to generate the pressure gradient. Consequently, the larger applied pressure leads to a larger pore pressure in the reservoir in the vicinity of the well-bore.

Figures 10–15 show the numerical results for the sustained stationary conductive fracture. Curves of the production rate q_{w} versus time for the two cases are plotted in Figure 10. In addition, the curves for the two cases based on the assumption that the procedure of crack growing and sand-filling is fulfilled instantly[5] are also plotted in Figure 10 for comparison. According to the assumption, the initial pore pressure in the medium is zero, but on the crack surface, it is uniformly distributed with the value $p^* = -\sigma_{22}^{\infty} + \Delta p - p_0$, where Δp is determined in such a way that it generates a stress intensity factor $K_I = K_{IC}$ at the crack tip as shown in the

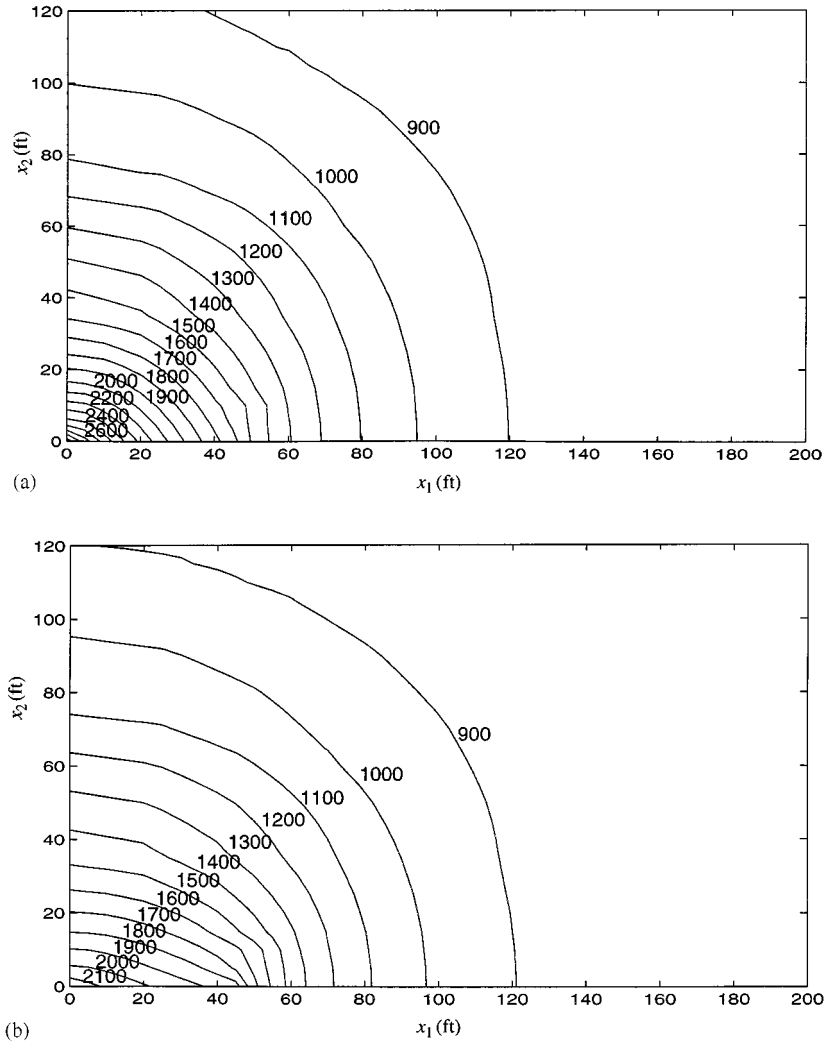

Figure 8. The transient pore pressure field (psi) at the crack length $L(t) = 47{\cdot}5$ ft (a) ($K_f = 1000\,K$, $\phi_f = 0{\cdot}15$); (b) ($K_f = 10\,000\,K$, $\phi_f = 0{\cdot}25$)

second sub-problem in Figure 4(a). The applied pressure at the well-bore is $p_w = -700$ psi. According to the convention made in the previous section, q_w is negative here. But it is treated positive for the curves plotting in Figure 10 so that the behavior of q_w can be elaborated conveniently. It is found that in the early stage, q_w for the scenario of gradually generated crack is larger than that for the scenario of instantly generated crack because the pore pressure in the reservoir for the former scenario is larger than that for the latter, and the width of the crack for the former scenario is larger than that for the latter also. After 1·2 days curves of q_w versus t for the two cases are close to each other gradually. However, one can imagine that if the crack growing and sand filling take a finite time, the medium in the vicinity of the crack must contain some

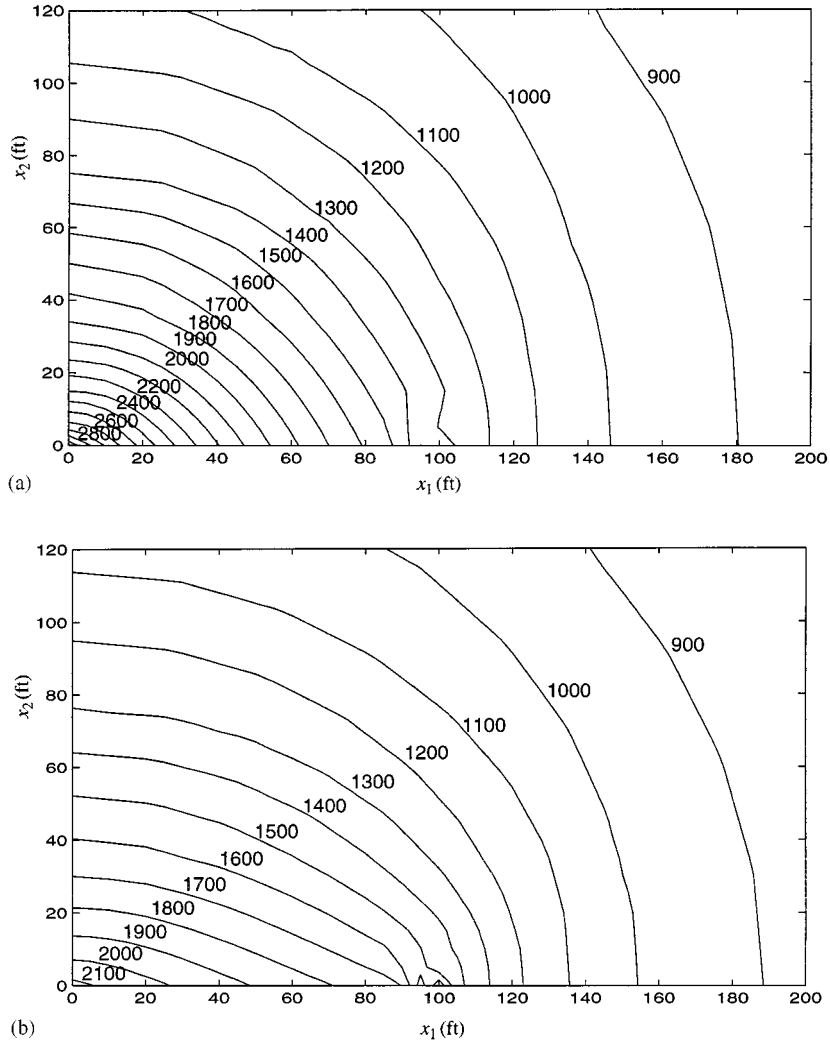

Figure 9. The transient pore pressure field (psi) at the half crack length $L(t) = 100$ ft (a) ($K_f = 1000\ K$, $\phi_f = 0{\cdot}15$); (b) ($K_f = 10\,000\ K$, $\phi_f = 0{\cdot}25$)

injected fluid. Therefore, in the early stage, the production rate q_w must include some injected fluid. As far as this fact is concerned, difference of the actual oil productivity in the early stage for the two scenarios may decrease. To evaluate the effectiveness of the conductive crack in raising the productivity, a curve of q_w versus t for a single well without conductive crack is also plotted in Figure 10. If the production rate for case 1 of a lower permeability crack-filling material is denoted by $q_w^{(1)}$, that for case 2 of a higher permeability crack-filling material by $q_w^{(2)}$, and that without the conductive fracture by $q_w^{(0)}$, it can be found that in the early stage, $q_w^{(1)}$ is nearly twice of $q_w^{(0)}$ and $q_w^{(2)}$ nearly triple of $q_w^{(0)}$. Even at the time $t = 1000$ days, $q_w^{(1)}$ is still nearly 1·2 times of $q_w^{(0)}$ and $q_w^{(2)}$ nearly 1·5 times of $q_w^{(0)}$.

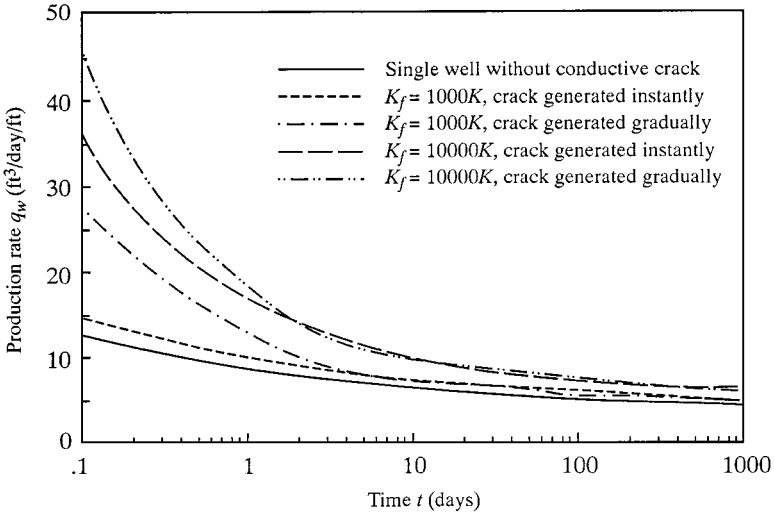

Figure 10. Curves of production rates q_w vs. time t for the stationary conductive fracture

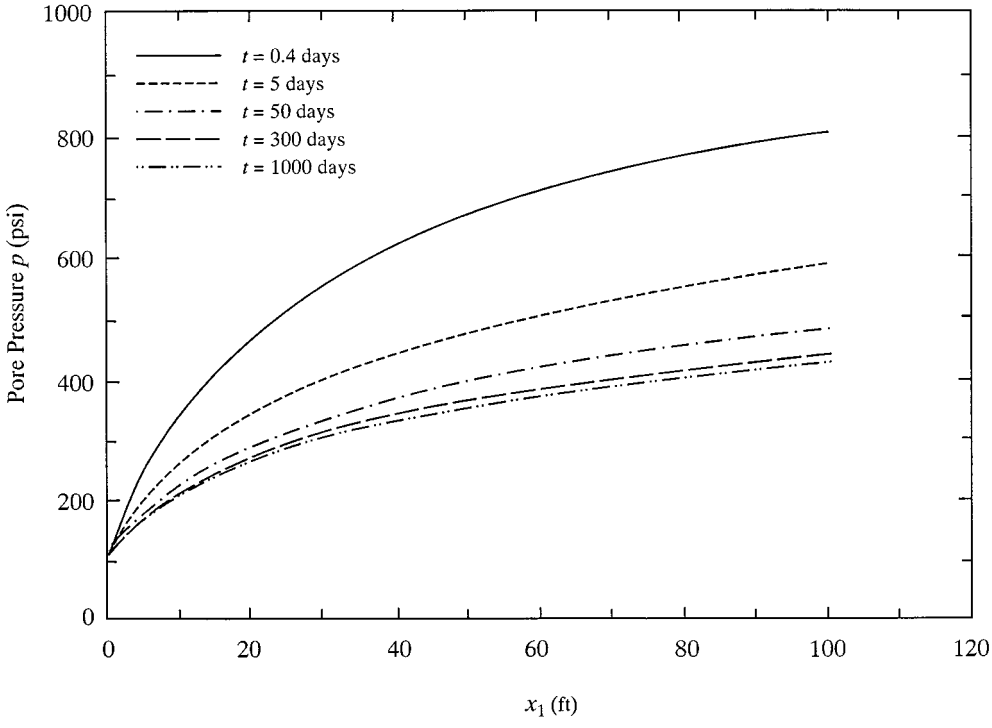

Figure 11. Distribution of the pore pressure in the stationary conductive fracture

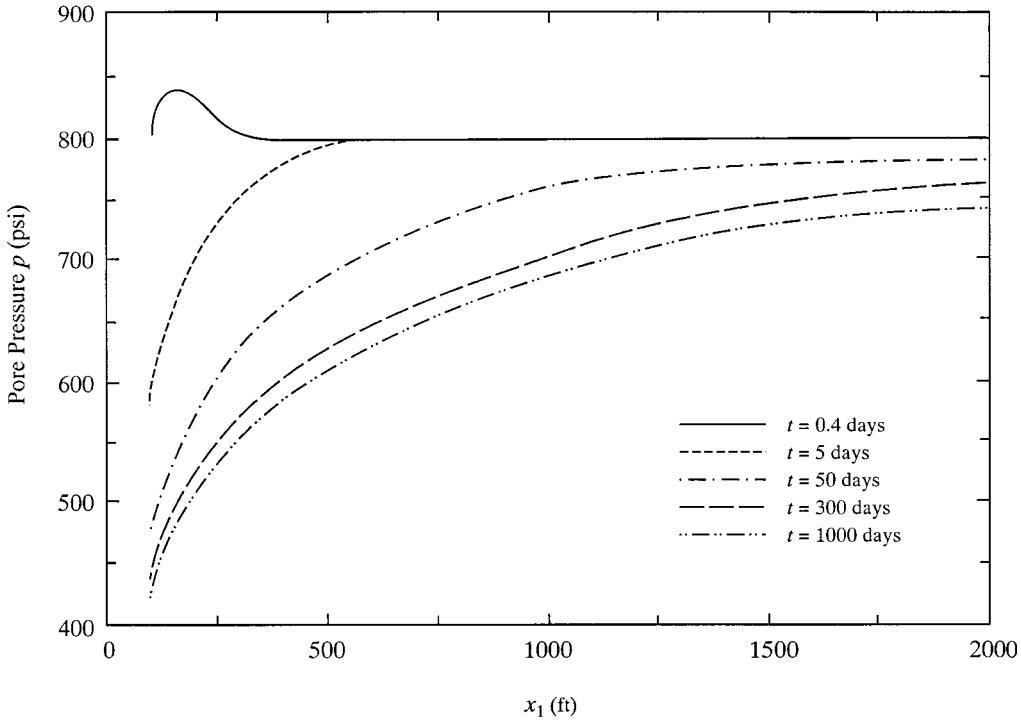

Figure 12. Distribution of the pore pressure on the x_1-axis

The pore pressure distributions on the x_1- and x_2-axes for case 1 are shown in Figures 11–13, which indicate that the pore pressure approaches its initial value p_0 when the material point gets further from the well. Figures 14 and 15 show the distributions of displacement components u_1 on the x_1-axis and u_2 on the x_2-axis, respectively, for case 1. In the early stage, magnitudes of u_1 and u_2 are small. In the later stage, as a result of the diffusion of the pore pressure, the displacements on the entire x_1- and x_2-axes have large magnitudes.

DISCUSSION ON CONDUCTIVITY COEFFICIENT

Cinco-Ley *et al.*[8] presented a definition of a dimensionless conductivity coefficient F_D for the rectangular stationary conductive fracture with an impermeable crack tip as

$$F_D = \frac{b_f K_f}{LK} \tag{56}$$

where b_f is the width of the rectangular conductive fracture. In engineering practice, if the conductive crack is considered to be formed by a hydraulic fracturing technique, the crack is not rectangular but elliptic. Crack width b_f can be defined as a nominal width such as the crack mouth opening displacement at the well-bore or the average value of the crack width. Whatever

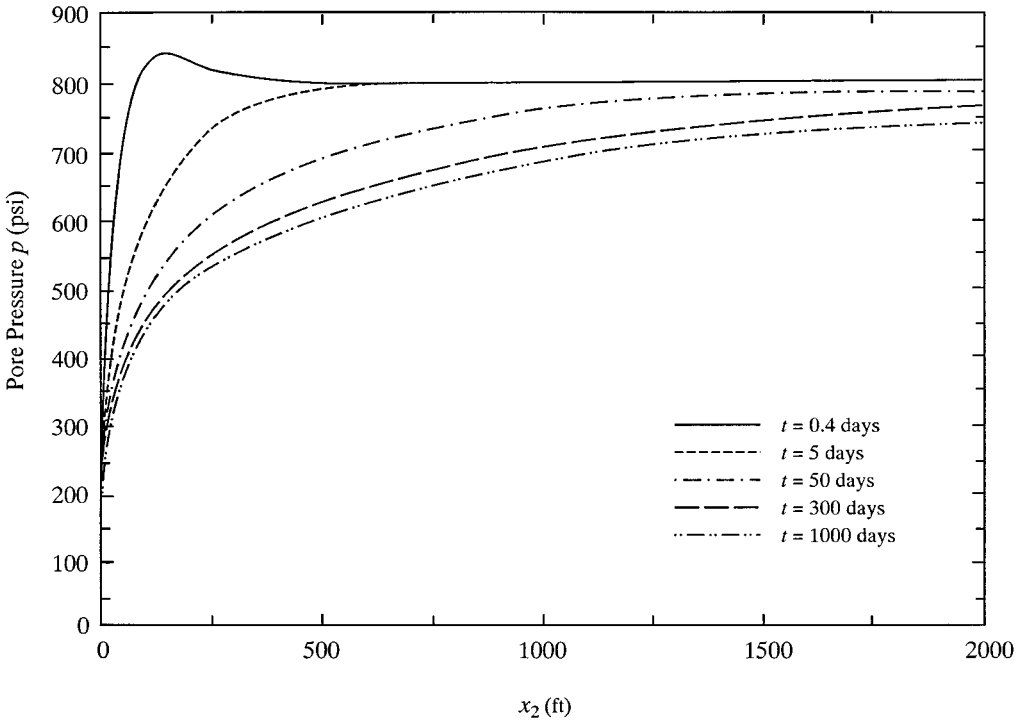

Figure 13. Distribution of the pore pressure on the x_2-axis

definition we have, b_f is dependent on the crack length, the elastic constants and the fracture toughness of the porous medium. Hence, a more reasonable definition of the dimensionless conductivity coefficient F_D for the stationary conductive fracture can be given as

$$F_D = \frac{1-v}{G}\frac{K_f}{K}\frac{K_{IC}}{\sqrt{L}} \tag{57}$$

The curves of production rates versus time for different conductivity coefficients F_D are plotted in Figure 16 for the example problem. The conductive fracture is considered to be generated instantly. As analyzed in the previous section, this model is still a good approximation. The curves for the two extreme cases $F_D = 0$ and $F_D = \infty$ are also plotted in Figure 16. For the case of a single well in the infinite medium without conductive fracture, we have $K_f = K$. It can be found that F_D resulting from equation (57) is an extremely small number. This is the case of $F_D = 0$. The case of $F_D = \infty$ means that the permeability coefficient of the crack-filling material is so large that the crack can be considered empty and the pressure is uniformly distributed on the crack surface and equal to the applied pressure at the well-bore. It is found in the computation that the curve for $F_D = 0{\cdot}1$ already coincides with that for $F_D = 0$ and the curve for $F_D = 100$ coincides with that for $F_D = \infty$. Due to the results, we can classify the conductive fracture into three categories: low conductivity fracture if $F_D < 0{\cdot}5$, medium conductivity fracture if $F_D = 0{\cdot}5$–5, and high conductivity fracture if $F_D > 5$. It is noted that when $F_D > 10$, raising the conductivity coefficient of the fracture is of little significance in increasing oil productivity.

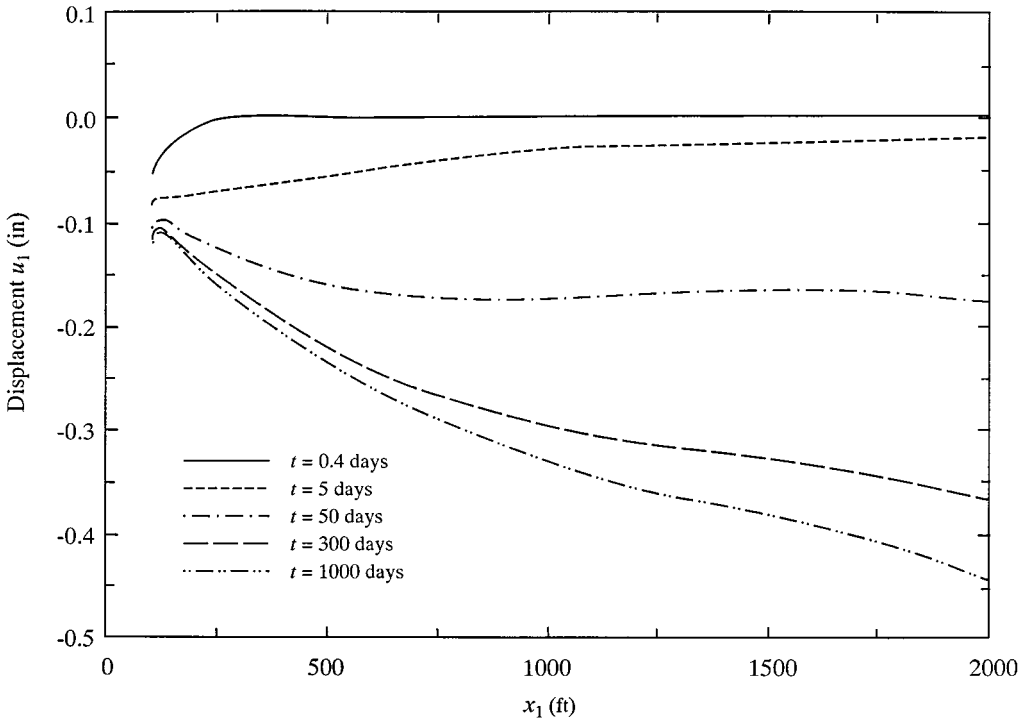

Figure 14. Distribution of the displacement components u_1 on the x_1-axis

CONCLUSIONS

In this study, the variational principle and the finite element method are presented for analyzing the transient deformation/seepage coupled problems for both a growing conductive fracture and a sustained stationary conductive fracture in an infinite poroelastic medium. The methodology associated with moving and relaying finite elements is found to be effective in the analysis of a growing conductive fracture in the medium. Numerical results for the example in the cases of $K_f = 1000$ K and $K_f = 10\,000$ K are provided. Results of the production rates for the example problem are compared with those of a single well in the infinite medium without the conductive fracture. A new definition of conductivity coefficient for stationary conductive fracture is recommended. Numerical results of the production rates for different conductivity coefficients are presented. The technique given here provides a quantitative estimation for the oil productivity when a hydraulically driven conductive fracture adjacent to the well-bore exists in the medium. The following conclusions can be drawn from the study:

1. For non-zero *in-situ* stress and non-zero initial pore pressure fields, the problem can be resolved into two sub-problems. One of them has the solution of uniform stress and pore pressure field and the other can be solved by means of the finite element method. The real solution of the problem can be obtained by superposition of the two sub-problems.

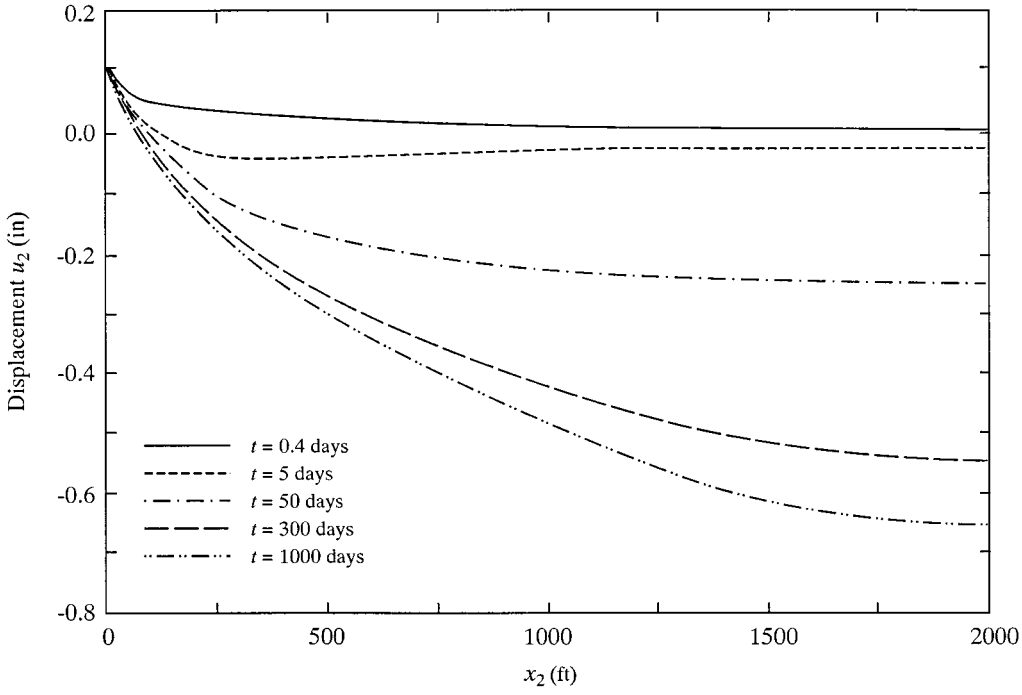

Figure 15. Distribution of the displacement components u_2 on the x_2-axis

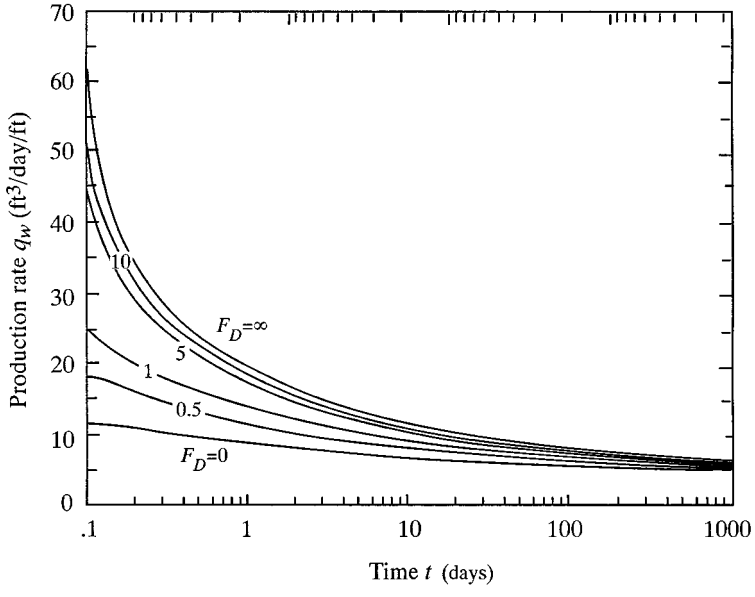

Figure 16. Curves of production rates vs. time for conductive fracture with different conductivity coefficients

2. For the problem of a well in an infinite domain with a conductive fracture, the infinite domain can be replaced by a sufficiently large elliptical domain, which is close to a circle, with the infinite elements laid in the region outside the finite domain. This method is proved accurate and efficient.
3. For the growing conductive fracture, the numerical results indicate that the injection rate, the applied pressure at the well-bore and the crack width at the well-bore oscillate with time because of the difference of the speeds between the crack propagation and the seepage flow. However, if the curves for these results are smoothed, we can find the tendency that the applied pressure at the well-bore increases in the initial time step and decreases thereafter, the injection rate at the well-bore decreases in the early stage and increases thereafter, and the crack width at the well-bore increases during crack propagation. For the sustained stationary conductive fracture with a prescribed constant applied pressure at the well-bore, the production rate decreases with increasing time.
4. The finite conductivity fracture adjacent to the well-bore in the oil formation is proved efficient in raising the oil productivity in primary recovery of oil fields. The conductive fracture can be classified into three categories according to the value of the conductivity coefficient F_D.

The applied pressure at the well-bore may vary with the vertical depth. Crack front may be curved rather than straight during the crack propagation. Friction may exist between the strata and the oil-bearing formation. Therefore, hydraulic fracturing is actually a three-dimensional problem. Nevertheless, the two-dimensional model study presented here provides us with some knowledge on the pore pressure and seepage flow in both the conductive fracture and the oil formation when the hydraulic fracturing technique is used. This knowledge may be helpful for the study of hydraulic fracturing in a three-dimensional model.

ACKNOWLEDGEMENTS

This work is sponsored by research grants, the Science Foundation G95(02) from State Education Commission of the People's Republic of China.

APPENDIX

English unit and their SI equivalents

Quantities	English units	SI equivalents
Length	ft	0·3048 m
	in	25·40 mm
Area	ft^2	0·0929 m^2
	in^2	645·2 mm^2
Volume	ft^3	0·0283 m^3
	in^3	16387·1 mm^3
Force	lb	4·448 N
	kip	4·448 kN
Pressure or stress	psf	47·88 Pa
	psi	6·895 kPa

REFERENCES

1. A. C. Gringarten, H. J. Ramey and R. Raghavan, 'Unsteady state pressure distributions created by a well with a single infinite conductivity vertical fracture', *Soc. Pet. Engng. J*., 347–360 (1974).
2. F. Kucuk and W. E. Brigham, 'Transient flow in elliptic systems', *Soc. Petrol. Engng. J*., 401–410 (1979).
3. H. Cinco-Ley, V. F. Samaniego and N. Dominguez, 'Transient pressure behavior for a well with finite conductivity fracture', *Soc. Petrol. Engng J*., 253–264 (1978).
4. Y. C. Li, 'Approximate analytical solutions for diffusion problems in unbounded media and their application in infinite elements', *Int. J. Numer Meth. Heat Fluid Flow*, **6,** 61–79 (1996).
5. Y. C. Li and N. C. Huang, 'Flow field modelling near a well with a conductive fracture', *Int. J. Numer Meth. Fluids*, **15,** 545–569 (1992).
6. D. A. Spence and P. Sharp, 'Self-similar solutions for elastohydrodynamic cavity flow', *Proc. Royal Soc. London*, *Ser. A*, **400,** 219–313 (1985).
7. N. C. Huang, A. A. Szewczyk and Y. C. Li, 'Self-similar solution in problem of hydraulic fracturing', *J. Appl. Mech.* **57,** 877–881 (1990).
8. N. C. Huang and Y. C. Li, 'Hydraulic fracturing with an impermeable crack', in Localized Damage, Computer-Aided Assessment and Control, Vol. 2, M. H. Aliabadi, C. A. Brebbia and D. J. Cartwright (eds), Computational Mechanics Publications, Southampton, Co-published with Springer, Berlin 1990, pp. 351–371.
9. K. Y. Lam and M. P. Cleary, 'Three-dimensional crack propagation under specified well-bore pressure', *Int. J. Numer. Analyt. Meth. Geomech*., **12,** 583–589 (1988).
10. T. J. Boone, and A. R. Ingraffea, 'A numerical procedure for simulation of hydraulically-driven fracture propagation in poroelastic media', *Int. J. Numer Analyt. Meth. Geomech*., **14,** 27–47 (1990).
11. M. A. Biot, 'General theory of three-dimensional consolidation', *J. Appl. Phys*., **12,** 155–164 (1941).
12. N. C. Huang, A. A. Szewczyk and Y. C. Li, 'Variational principles and finite element method for stress analysis of porous media', *Int. J. Numer Analyt. Meth. Geomech*., **14,** 1–26 (1990).
13. J. Ghaboussi and E. L. Wilson, 'Flow of compressible fluid in porous media', *Int. J. Numer. Meth. Engng*., **5,** 419–442 (1973).
14. J. R. Rice and D. M. Tracey, '*Computational fracture mechanics*', in Numerical and Computer Methods in Structural Mechanics, S. J. Fenves, N. Perrone, A. R. Robinson and W. C. Schnobrich (eds), New York, Academic Press, 1973, pp. 585–623.
15. P. P. Lynn and H. A. Hadid, 'Infinite elements with $1/r^n$ type decay', *Int. J. Numer. Meth. Engng* **17,** 347–355 (1981).
16. M. L. Williams, 'On the stress distribution at the Base of a stationary Crack', *J. Appl. Mech*., **24,** 109–114 (1957).
17. S. K. Chen, I. S. Tuba and W. K. Wilson, 'On the finite element method in linear fracture mechanics', *Engng. Fracture Mech*., **2,** 1–17 (1970).

